

Automated Detection of Solar Radio Bursts using a Statistical Method

Dayal Singh ¹ · K. Sasikumar Raja ^{1,2} ·
Prasad Subramanian ¹ · R. Ramesh ³ ·
Christian Monstein ⁴

© ●●●●

Abstract Radio bursts from the solar corona can provide clues to forecast space weather hazards. After recent technology advancements, regular monitoring of radio bursts has increased and large observational data sets are produced. Hence, manual identification and classification of them is a challenging task. In this paper, we describe an algorithm to automatically identify radio bursts from dynamic solar radio spectrograms using a novel statistical method. We used e-CALLISTO radio spectrometer data observed at Gauribidanur observatory near Bangalore in India during 2013 - 2014. We have studied the classifier performance using the receiver operating characteristics. Further, we studied type III bursts observed in the year 2014 and found that 75% of the observed bursts were below 200 MHz. Our analysis shows that the positions of the flare sites which are associated with the type III bursts with upper frequency cut-off $\gtrsim 200$ MHz

✉ K. Sasikumar Raja
sasikumarraja@gmail.com

Dayal Singh
dayal.singh@students.iiserpune.ac.in

Prasad Subramanian
p.subramanian@iiserpune.ac.in

R. Ramesh
ramesh@iiap.res.in

Christian Monstein
monstein@irsol.ch

- ¹ Indian Institute of Science Education and Research, Pashan, Pune - 411 008, India
- ² Physical Research Laboratory, Navrangpura, Ahmedabad-380 009, India.
- ³ Indian Institute of Astrophysics, 2nd Block, Koramangala, Bangalore - 560 034, India.
- ⁴ Istituto Ricerche Solari Locarno (IRSOL), Via Patocchi - Prato Pernice, 6605 Locarno Monti, Switzerland.

originate close to the solar disk center.

Keywords: Corona, Radio Emission; Radio Bursts; Instrumentation and Data Management

1. Introduction

Radio bursts from the Sun play an important role in understanding solar atmosphere, solar wind, and particularly coronal mass ejections. Many of these bursts provide clues to understand space weather. Radio bursts are observed over a wide range of frequencies (from few GHz to kHz), and they help to probe the solar atmosphere from chromospheric heights to 1 AU and beyond. Based on their morphology and frequency drift speeds (drift rates) in the dynamic spectrograms, they are classified into five primary types viz. Type I, Type II, Type III, Type IV and Type V bursts (Wild, 1967). Type J and Type U are the other complex bursts which are often observed in the solar corona (Kundu, 1965; McLean and Labrum, 1985).

Technology advancements have enabled us to observe solar radio bursts with sophisticated telescopes both from ground and space. For example, some ground based solar dedicated radio spectrographs are: Radio Solar Telescope Network (RSTN) operated by US airforce (Guidice *et al.*, 1981), Gauribidanur Low frequency Solar Spectrograph (GLOSS) in India (Kishore *et al.*, 2014), Hiraiso Radio Spectrograph (HiRAS) in Japan (Kondo *et al.*, 1994), IZMIRAN in Russia (Gorgutsa *et al.*, 2001), ARTEMIS-IV in Greece (Caroubalos *et al.*, 2001) and many others¹. Apart from these, there are more than 150 observing stations setup around the world to monitor the Sun, 24 hours a day. Presently about 52 of them regularly upload/provide data to a server at the University of Applied Sciences (FHNW) in Brugg/Windisch, Switzerland. The data processing is managed at Swiss Federal Institute of Technology (ETH) in Zurich, Switzerland. All these stations jointly constitute the e-CALLISTO network² (Benz *et al.*, 2009; Sasikumar Raja *et al.*, 2018). Space based observations at $\lesssim 14$ MHz are carried out using WAVES-WIND (Bougeret *et al.*, 1995), and WAVES-STEREO (Kaiser, 2005; Rucker *et al.*, 2005) instruments. There are attempts to combine these space-based observations with the ground-based observations also (see for example Hariharan *et al.* (2016)). All these spectrometers produce large datasets. For instance, in the present work, we used data observed using the CALLISTO spectrometer located at Gauribidanur observatory, India (Monstein, Ramesh, and Kathiravan, 2007) that recorded ≈ 13000 files in two years. Therefore, manual identification of the radio bursts is not possible - hence the present work.

In recent times, machine learning applications are widely used in classification problems. It is known that, if we want to apply them to classify various types

¹https://www.astro.gla.ac.uk/users/eduard/cesra/?page_id=187

²<http://www.e-callisto.org/>

of solar radio bursts, the machine needs to be ‘trained’ and we need large set of data for each type of burst. As mentioned previously, manual identification of bursts in a training dataset is an onerous task. We also know that more the training data, better the performance of classifier (classification method). Hence, in this paper, we present an algorithm to automatically identify the radio bursts using a statistical method. The developed algorithm could detect whether or not there is a radio burst present in the spectrogram. Our primary motivation is to use the database prepared using the algorithm described in the paper, and develop an automated classifier which would classify various types of individual bursts. So far, there have attempts to automatically identify specific type of bursts (Lobzin *et al.*, 2009, 2010; Lobzin, Cairns, and Zaslavsky, 2014; Salmane *et al.*, 2018; Zhang, Wang, and Ye, 2018). However, automatic recognition of all types of bursts was never reported in the literature to the best of our knowledge.

In this paper, § 2 describes the observational details of the data used. In § 3, a novel statistical method to automatically identify the radio bursts is explained. § 4 describes the performance of the algorithm using the receiver operating characteristics and analysis of all type III bursts observed in the year 2014. The summary, conclusion and future scope are discussed in § 5.

2. Observations

The observations of e-CALLISTO spectrometers began in the year 2009. Since then, so far > 150 stations are installed around the globe as previously mentioned. Most of the stations use the log-periodic dipole antenna (LPDA) as the primary receiving element (see for example Kishore *et al.* (2014); Sasikumar Raja *et al.* (2013a)). The e-CALLISTO receiver is designed to operate over the bandwidth 45-870 MHz. But different e-CALLISTO stations operate over different user selected radio windows based on the local conditions. For this study, we used the data observed at Gauribidanur observatory, located at longitude $77^{\circ} 27' 07''$ E, latitude $13^{\circ} 36' 12''$ N and ≈ 694 meters above sea level (Ebenezer *et al.*, 2007; Ramesh, 2011; Kishore *et al.*, 2015). At Gauribidanur observatory, spectral radio observations of the Sun with the e-CALLISTO are carried out everyday during 02:30 - 11:30 UT. The frequency range of operation is 45-450 MHz. The observed data, about 400 frequencies per sweep, are stored as FITS-files. The time resolution of the instrument is 0.25 sec at the rate of 200 channels per spectrum (i.e. 800 pixels/sec). The integration time is 1 msec and the radiometric bandwidth is about 300 kHz. The overall dynamic range of the e-CALLISTO is > 50 dB.

Statistically, the number of radio bursts observed during the solar maximum are larger (in comparison to the solar minimum). Therefore, we selected the years 2013 and 2014 (solar maximum of solar cycle 24) for this study. The detailed method and results are discussed in the subsequent sections.

3. Method

In order to classify the radio bursts, the basic observed parameters used from the dynamic spectrograms are area, slope, relative intensity, start and end time of

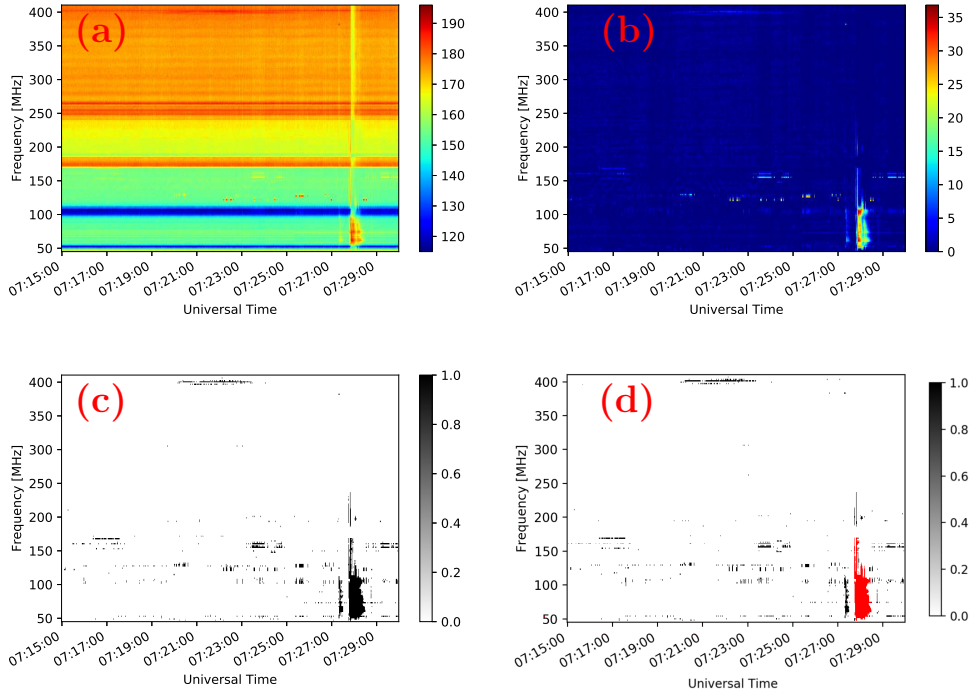


Figure 1. Various stages of processing the spectrogram observed at Gauribidanur observatory on 04 January 2013 are shown. Panel (a) shows the raw spectrogram; panel (b) is the spectrogram after the background subtraction; panel (c) is the binary image of the spectrogram in panel (b); the region shown in red in panel (d) indicates the burst identified by the classifier discussed in the paper.

the bursts, and the frequency range over which they were observed. We carefully inspected the above parameters to identify the radio bursts. The terrestrial radio frequency interference (RFI) appear as continuous features in dynamic spectra (for example FM, television, satellite signals, etc.); in some cases they appear as sharp pulses. By contrast, solar radio bursts drift as they propagate from high to low frequencies. We identify and eliminate the RFI making use of this key difference between RFI and radio bursts. The drift rate of the radio bursts can be measured using the Equation 1. This is one of the main parameters which we use to identify solar radio bursts from the data. Figure 1 shows the spectrogram observed on 04 January 2013. Panel (a) shows the observed raw spectrogram (before processing). We calculate the median over time for every frequency channel and the resultant column matrix is subtracted from every column of the raw data corresponding to the spectrogram shown in panel (a). After median filtering (background subtraction) most of the continuous local RFI were eliminated (see panel (b)). We repeated this process for the entire dataset observed in the year 2013 (Set-P). We found the standard deviation (i.e. 1σ) of the entire processed Set-P to be 0.6 dB. We selected the $5\sigma = 3$

dB as the initial cut-off to identify whether or not there is a solar radio burst present in the frame. To reduce complexity, we converted every processed image to a binary image; i.e., if the signal is greater than 3 dB count we assigned the number one; else the number is zero. The binary image is shown in panel (c). Using the binary images, contours of the images were traced using the ‘`opencv`’ python library and measured the area (A_c) and coordinates of the contours. In the e-CALLISTO spectrometers, channels with high RFI are avoided due to practical reasons. Therefore, in the cases where the radio bursts intercept the RFI band, our algorithm underestimates the area. For instance, at Gauribidanur observatory, the FM band ($\approx 87 - 109$ MHz) was not used and therefore, the measured A_c was underestimated by a factor $\approx 22 \times$ duration of the radio burst. However, this factor does not significantly impact our results.

By knowing the coordinates, we calculated the slope (v_d , also called f-t range ratio) of the radio bursts using

$$v_d = \frac{\Delta f}{\Delta t} = \frac{f_2 - f_1}{t_2 - t_1} \quad (1)$$

where f_2 and f_1 are the maximum and minimum frequencies respectively, t_2 , t_1 are the start and end times of the radio burst. As previously described, most of the RFI appear as horizontal and vertical lines. They are successfully eliminated by selecting the v_d in the range $0.81 \text{ MHz s}^{-1} < v_d < 162 \text{ MHz s}^{-1}$.

We find that A_c and v_d alone are not sufficient to automatically identify the bursts. The area depends on the bandwidth and duration of the observed burst. At the same time, we found that the drift rate can mislead the algorithm for smaller Δf and Δt . Therefore, we defined a new parameter called the Area Slope Index (ASI):

$$ASI = A_c \times v_d \quad (2)$$

If the maximum ASI measured for each file is greater than a certain threshold, we conclude that there is at least one solar radio burst present in the image. If the ASI is less than threshold, we conclude that no significant solar radio burst is present in the image.

In order to decide the ASI threshold, we manually separated the bursts observed in the year 2013 and named it as Set-B. We measured the probability of finding the number of bursts for a given ASI value ($P_B(ASI)$), for Set-B using

$$P_B(ASI) = \frac{N_B(ASI)}{N_{TB}}, \quad (3)$$

where $N_B(ASI)$, N_{TB} are the number of bursts for a given ASI and the total number of bursts in Set-B respectively.

Similarly, using the complete dataset observed in 2013 (Set-U, that includes the data with bursts and without bursts), we defined another parameter,

$$P_U(ASI) = \frac{N_U(ASI)}{N_{TU}}, \quad (4)$$

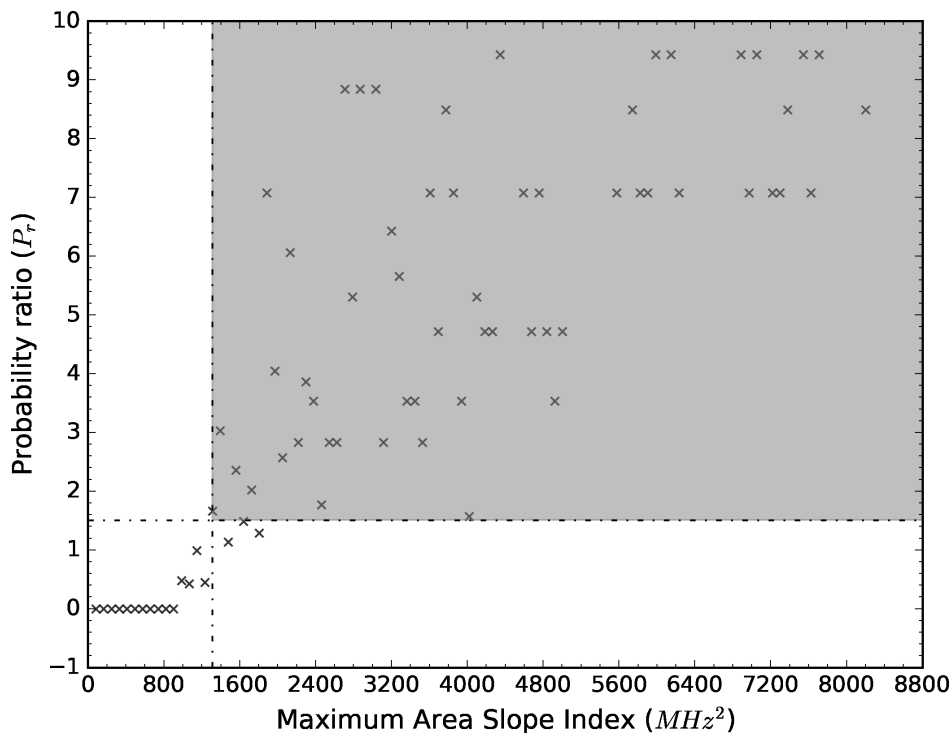


Figure 2. Variation of the probability ratio (P_r) with the ASI is shown. The horizontal and vertical ‘dash dot’ lines denote $P_r = 1.5$ and $ASI \approx 1312 \text{ MHz}^2$. The points in the gray shaded region with $P_r \gtrsim 1.5$ and $ASI \gtrsim 1312 \text{ MHz}^2$ indicate the presence of at least one radio burst in the spectrogram. There are no bursts present in the white region. $P_r = 0$ indicates that there were no images with at least one radio burst present in it for the corresponding ASI value.

where $N_U(ASI)$, N_{TU} are the number of bursts for given ASI and the total number of bursts in the Set-U respectively.

The ratio of equations 3 and 4 (which gives P_r , the probability ratio) for different ASI is calculated using

$$P_r(ASI) = \frac{P_B(ASI)}{P_U(ASI)}, \quad (5)$$

The probability ratio is then plotted with respect to ASI as shown in Figure 2. From Figure 2, we find that $P_r = 1.5$ corresponds to an $ASI \approx 1312 \text{ MHz}^2$. As mentioned in the flowchart (Figure 3), if the ASI is greater than the cut-off value of 1312 MHz^2 , we conclude that the corresponding image has at least one solar radio burst. Otherwise, there is no burst present in the image. We used this method to identify all the solar radio bursts in the years 2013 and 2014. We note here that for certain ASI values, there might be no images with radio bursts present - hence the value P_r is zero as seen in Figure 2.

Radio emission from the ‘quiet’ Sun component remains relatively constant throughout the solar cycle. The slowly varying component varies with the solar

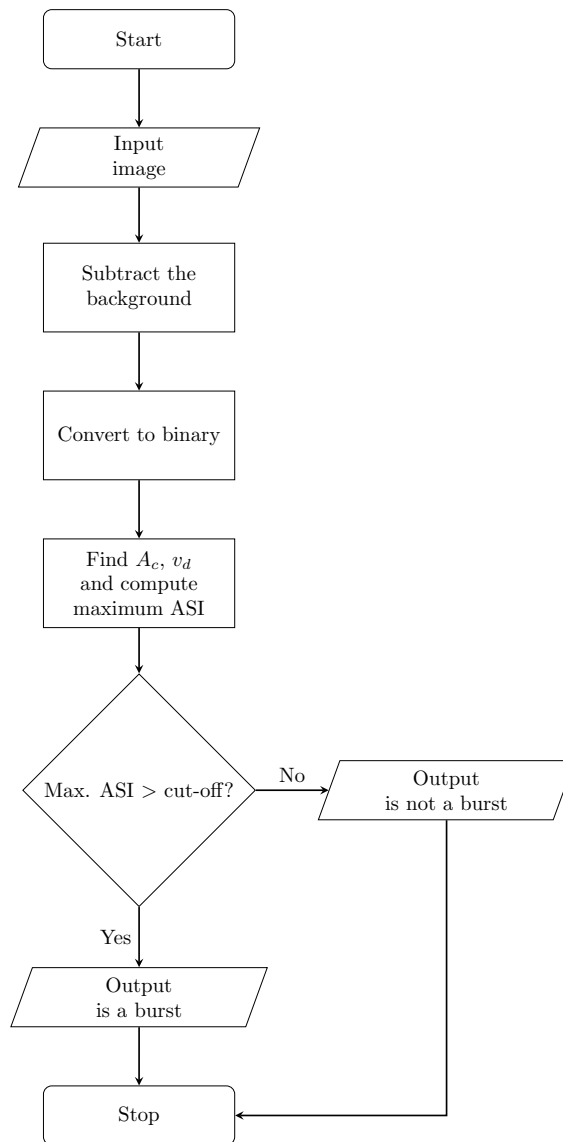


Figure 3. The flow chart shows an algorithm to identify whether or not the input file has the radio emission.

cycle, but this is mostly observed at microwave frequencies. Due to sensitivity limitations neither the quiet Sun, nor the slowly varying components of radio emission can be observed using e-CALLISTO. The non-thermal radio bursts are easily observed with the e-CALLISTO, since they are comparatively stronger. Furthermore, although the occurrence rate of solar radio bursts varies with solar cycle, their characteristic properties (i.e. v_d , bandwidth and duration of the radio burst) vary only minimally. Therefore the ASI cut-off (which depends on

v_d , bandwidth and duration of the radio burst) remains unchanged throughout the solar cycle. The performance of the classifier is discussed in the § 4.

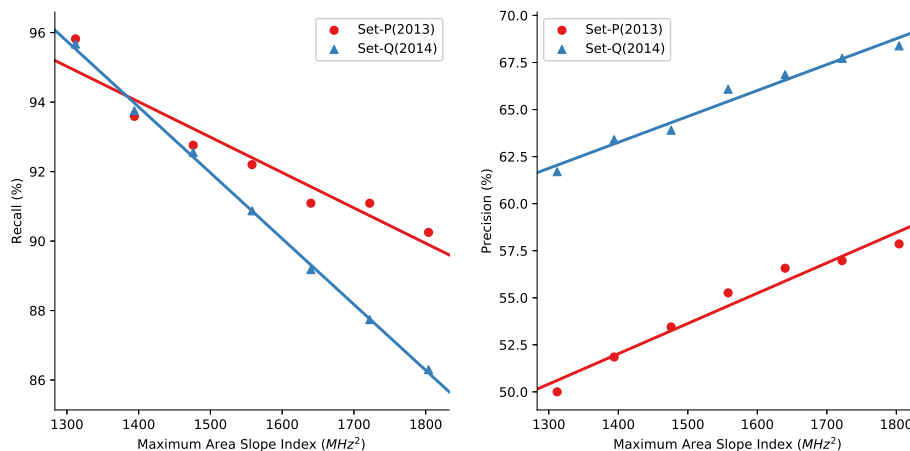


Figure 4. The ROC parameters: recall (left panel) and precision (right panel) are shown for different ASI. The red and blue circles and triangles indicate the years 2013 (Set-P) and 2014 (Set-Q).

4. Results and Discussions

4.1. Performance of the algorithm

We processed the raw data and identified the radio bursts using the method described in the § 3 and Figure 3. Using the receiver operating characteristics (ROC), we studied the performance of the classifier (Fawcett, 2006). Herewith, we summarize the necessary terms for the sake of completeness. If the instance is positive and it is classified as positive then it is termed as ‘true positive’. If the instance is negative and is classified as positive, then it is called ‘false positive’. By manually counting these parameters in the classified dataset (by the algorithm), we measured the ‘true positive’ rate (tp rate or recall) using

$$\text{tp rate} = \frac{\text{TP}}{\text{P}} \quad (6)$$

where TP and P are the positives correctly classified and the total number of positive instances.

We also measured the ‘false positive’ rate (fp rate or false alarm rate) of the classifier using

$$\text{fp rate} = \frac{\text{FP}}{\text{N}} \quad (7)$$

Table 1. Variation of recall and precision of the Set-P and Set-Q for different Area Slope Indices.

S. No.	ASI (MHz ²)	Set-P		Set-Q	
		Recall	Precision	Recall	Precision
(1)	(2)	(3)	(4)	(5)	(6)
1	1312	95.82	50.00	95.67	61.70
2	1394	93.59	51.85	93.75	63.40
3	1476	92.76	53.45	92.55	63.90
4	1558	92.20	55.26	90.87	66.08
5	1640	91.09	56.57	89.18	66.85
6	1722	91.09	56.97	87.74	67.72
7	1804	90.25	57.86	86.30	68.38

where FP and N are negatives incorrectly classified and the total negative number of instances.

By knowing the tp rate and fp rate (see Equations 6 and 7), we calculated the recall and precision using

$$\text{Recall} = \frac{\text{TP}}{\text{P}} \quad (8)$$

$$\text{Precision} = \frac{\text{TP}}{\text{TP} + \text{FP}} \quad (9)$$

Note that the high value of recall and precision indicate the small number of ‘false negatives’ (i.e., where the instance is positive and classified as negative) and ‘false positives’ respectively. The calculated values of recall and precision for different ASI cut-offs are tabulated in Table 1. In the year 2013, for the significant ASI (i.e., 1312 MHz²), the calculated recall and precision are 95.82% and 50% respectively. The recall and precision for the dataset observed in 2014 (Set-Q, for the same ASI value) are 95.67% and 61.7% respectively. The recall and precision for different ASI values are shown in Figure 4. It shows that the parameter recall is more or less consistent for both Set-P and Q. However, the precision shows a difference of 12% between Set-P and Q. We found that the improved precision in the year 2014 is due to the reduced RFI and the availability of the dataset.

4.2. Preliminary analysis of Type III bursts

We carried out a preliminary analysis of all the type III bursts detected during the year 2014 using the automatic detection method described in this paper. We found a total of 238 type III bursts during our observing period (\approx 02:30 - 11:30 UT). Out of the above, 88 type III bursts were associated with GOES

soft X-ray and/or Halpha flares^{3, 4, 5, 6}. Note that we define a type III burst to be flare associated if it occurred during the onset-end phase of the flare. The observational details of the Type III bursts and associated flares are provided in Appendix (see Table 2). The remaining 150 type III bursts were not associated with any flare. These 150 bursts were probably due to weak energy releases in the solar atmosphere reported earlier in the literature (for example, Ramesh *et al.* (2010, 2013); Saint-Hilaire, Vilmer, and Kerdraon (2013); Sasikumar Raja and Ramesh (2013b); Mugundhan, Hariharan, and Ramesh (2017); James, Subramanian, and Kontar (2017); James and Subramanian (2018); Sharma, Oberoi, and Arjunwadkar (2018)).

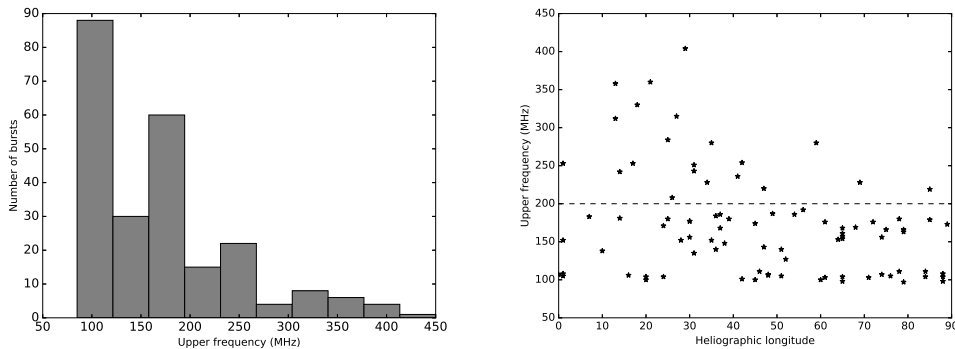


Figure 5. **LEFT:** The number of type III bursts observed (with and without flares) as a function of their upper frequency cut-off. **RIGHT:** The distribution of upper frequency cut-offs of the flare associated type III bursts (in the LEFT panel) with respect to the heliographic longitudes of the associated flare. The bursts whose upper frequencies are greater than 200 MHz are separated by a dashed line.

We also find that 75% of the type III bursts in our list were observed below 200 MHz (left panel of Figure 5). An inspection of the source region of the associated flares indicate a pattern. While the flare locations are uniformly distributed between 0° and 90° longitude for bursts with upper frequency cut-off < 200 MHz, they are limited to $0^\circ - 50^\circ$ longitude for bursts with upper frequency cut-off > 200 MHz (see right panel of Figure 5). This seems to indicate that bursts with higher starting frequencies are more directive. A detailed investigation of these results (using more data) will be reported elsewhere.

³https://cdaw.gsfc.nasa.gov/CME_list/NOAA/org_events_text/

⁴https://www.ngdc.noaa.gov/stp/space-weather/solar-data/solar-features/solar-flares/x-rays/goes/xrs/goes-xrs-report_2014.txt

⁵http://www.lmsal.com/solarsoft/ssw/last_events-2014/

⁶http://hec.helio-vo.eu/hec/hec_gui.php

5. Summary and Conclusions

In this paper, we have presented an automated method to detect solar radio bursts. Although this method doesn't classify the types of radio bursts, it is able to discriminate between dynamic spectra with and without solar radio bursts. Our algorithm can operate with all standard image formats and does not need FITS files. The method is tested on two years of e-CALLISTO data observed at Gauribidanur observatory. Using this method, we have identified 1182 radio bursts during January 2013 - April 2018. The list of these bursts can be found at (<http://www.iiserpune.ac.in/~p.subramanian/Bursts.zip>). Furthermore, we studied all type III bursts observed in the year 2014 and found that 75% of the bursts observed were below 200 MHz. The source region of the associated flares were close to the disk center (i.e. heliographic longitude $0^\circ - 50^\circ$) for bursts with upper frequency cut-off > 200 MHz (Figure 5).

We have defined an Area Slope Index (ASI) and found that the dynamic spectra images with $ASI \gtrsim 1312 \text{ MHz}^2$ have at least one solar radio burst. Using this ASI threshold, the recall for this method is over 95% and the precision is between 50 and 61%. The precision and recall for different ASI values are shown in Figure 4. The precision of the method can be improved (at the cost of poor recall by increasing the ASI cut-off) and vice versa. The precision can also be improved by comparing with the observations at other e-CALLISTO stations. One of the drawbacks of this method is that the weak radio bursts whose SNR is $< 5\sigma$ are insensitive to this method. Better data (which can allow for a lower SNR cutoff) can overcome this drawback.

A successful classifier with good performance can play a crucial role in understanding properties of solar radio bursts like drift rates, spectral indices and emission mechanisms, which are in turn are very useful in solving long-standing solar physics problems associated with coronal heating, propagation of coronal mass ejections and others. For instance, it is known that some kinds of radio bursts (such as Type II and Type IV) correlate with the geomagnetic storms, auroras and other space weather effects.

Accordingly, we plan to develop an automated burst classifier (that can discriminate between different kinds of bursts) in the future. We know that more the number of training datasets, better the performance of the classifier. However, this is a challenge by way of data processing. Since the e-CALLISTO stores one frame every 15 min and since observations are carried out for ≈ 9 hours per day, it produces ≈ 65000 files in 5 years. Therefore, a 52 station e-CALLISTO network produces > 3.37 million files in 5 years. Each file size is ≈ 700 kB. The file sizes are expected to be much higher for digital back end instrumentation based on FPGAs and fast ADCs (see for example Kumari *et al.* (2017); Mugundhan *et al.* (2018)). Hence the necessity of a sophisticated algorithm to classify solar radio radio bursts. We would remark here that, there are another type of short duration (< 0.1 s) spike bursts (for e.g., Tarnstrom and Philip (1972)) with a small area are difficult to identify using the reported algorithm. In the future, we would like to develop an algorithm which would identify such bursts by cross-comparing the dynamic spectrograms observed by different observatories (which would help in mitigating local RFI). Such an algorithm can not only identify spike bursts, but also improve the efficiency of the scheme reported in this paper.

Acknowledgment DS acknowledges the INSPIRE-SHE program of Department of Science & Technology, India. KSR acknowledges the financial support from the Science & Engineering Research Board (SERB), Department of Science & Technology, India (PDF/2015/000393). KSR acknowledges the NVIDIA Corporation for supporting this project by donating the Titan Xp GPU. The authors would like to thank the anonymous referee for his/her comments that helped in improving the manuscript.

Appendix

Details of flare associated solar radio Type III bursts mentioned in Section 4.2 are listed in Table 2.

Table 2.: Flare associated Type III bursts observed using Gauribidanur e-CALLISTO during 2014.

S. No. (1)	Date (2)	Type III bursts			Flares				
		Start time (UT) (3)	Frequency (MHz)		Time (UT)		Class (8)	Active region (9)	Location (10)
			Start (4)	Stop (5)	Onset (6)	End (7)			
1	20140101	7:25:14	47	143	07:21	07:29	C	11940	S12W47
2	20140126	8:28:44	45	219	08:26	09:33	C	11967	S14E85
3	20140126	10:07:31	45	171	10:05	10:19	C	11960	S15W24
4	20140129	4:16:44	45	157	04:06	04:42	C	11967	S12E65
5	20140129	6:54:50	45	161	06:53	07:34	C	11967	S12E65
6	20140129	7:00:25	45	98	06:53	07:34	C	11967	S12E65
7	20140129	7:28:47	45	168	06:53	07:34	C	11967	S12E65
8	20140130	7:53:54	45	127	07:54	08:41	M	11967	S12E52
9	20140131	5:32:56	45	168	04:46	05:17	C	11967	S14E37
10	20140210	5:03:01	45	177	05:04	05:23	C	11974	S12E30
11	20140215	8:24:09	45	148	08:25	08:39	C	11974	S13W38
12	20140303	7:22:29	45	135	07:10	07:19	C	11989	N07W31
13	20140415	7:06:00	45	315	07:04	07:11	C	12035	S15E27
14	20140415	9:16:07	45	284	09:15	09:25	C	12035	S14E25
15	20140416	3:20:38	45	106	03:03	03:16	C	12035	S15E16
16	20140416	4:15:03	45	163	04:11	04:14	C	12042	N19E79
17	20140416	5:01:50	45	181	04:57	05:14	C	12035	S15E14
18	20140416	5:15:00	45	242	04:57	05:14	C	12035	S15E14
19	20140416	5:34:13	45	111	05:21	05:38	C	12042	N19E78
20	20140416	6:37:11	45	358	06:37	06:48	C	12035	S17E13
21	20140416	6:44:04	45	312	06:37	06:48	C	12035	S17E13

Continued on next page

Table 2 – continued from previous page

S. No. (1)	Date (2)	Type III bursts			Flares				
		Start time (UT) (3)	Frequency (MHz)		Time (UT)		Class (8)	Active region (9)	Location (10)
			Start (4)	Stop (5)	Onset (6)	End (7)			
22	20140416	7:16:59	45	253	07:17	07:26	C	12034	N03W01
23	20140416	8:19:42	45	152	08:12	08:20	C	12034	N03W01
24	20140416	8:48:38	45	166	08:36	08:51	C	12035	N19E75
25	20140419	9:18:44	45	105	09:17	09:22	C	2032	N12W76
26	20140419	9:25:00	45	254	09:24	09:29	C	2036	S15W42
27	20140501	4:06:00	45	180	03:58	04:04	B	12048	N19W78
28	20140506	8:49:46	45	104	08:41	09:21	M	12051	S15W84
29	20140604	7:20:52	45	105	07:07	07:16	B	12080	S11E51
30	20140611	4:40:50	45	103	04:39	04:56	C	12087	S12E71
31	20140611	5:31:15	45	152	05:30	05:36	M	12080	S12W35
32	20140611	7:07:46	45	140	07:09	07:15	C	12080	S12W36
33	20140611	8:58:06	45	104	08:59	09:10	X	12087	S18E65
34	20140613	7:44:00	45	105	07:49	07:59	M	12089	N18W01
35	20140613	7:50:30	45	108	07:49	07:59	M	12089	N18W01
36	20140613	9:14:28	45	236	09:14	09:20	C	12087	S17E41
37	20140613	9:16:20	45	180	09:14	09:20	C	12087	S18E39
38	20140617	6:29:04	45	183	06:29	06:31	B	12087	S20W07
39	20140617	7:38:40	45	154	07:36	07:46	B	12085	S23W65
40	20140617	8:22:55	45	103	08:13	08:49	C	12093	S11E61
41	20140617	10:07:01	45	169	09:59	10:05	B	12085	S22W68
42	20140625	7:57:44	45	101	07:53	08:26	B	12096	N09E42
43	20140628	7:35:57	45	173	07:36	07:49	C	12104	S12E89
44	20140630	6:51:43	45	100	06:52	07:10	C	12100	N09E20
45	20140630	7:04:16	45	104	06:52	07:10	C	12100	N09E20
46	20140702	6:56:33	53	100	06:41	06:49	C	12106	N15E45
47	20140702	7:39:07	53	153	07:34	07v38	C	12108	S08E64
48	20140702	10:50:03	53	152	10:26	10:58	C	12102	N15E28
49	20140708	2:31:09	54	98	02:31	02:36	C	12114	S19E88
50	20140708	5:30:00	45	100	05:31	05:39	C	12113	N09E60
51	20140709	4:37:42	51	176	04:37	04:39	C	12114	S12E61
52	20140709	6:17:00	45	107	05:29	06:12	C	12113	N11E48
53	20140723	7:28:02	45	228	07:28	07:51	B	12121	N07E69
54	20140724	9:24:06	45	192	09:10	09:17	B	12121	N08E56
55	20140725	6:58:50	45	280	06:57	07:07	C	12121	N11E35
56	20140731	4:39:22	45	156	04:39	05:09	B	12127	S05E30
57	20140810	6:41:42	45	138	06:44	06:52	B	12137	S18W10
58	20140811	6:16:52	45	104	06:21	06:27	B	12137	S17W24
59	20140811	10:07:26	45	208	10:09	10:12	B	12137	S19W26
60	20140905	6:50:42	45	174	06:16	07:18	C	12152	S13W45

Continued on next page

Table 2 – continued from previous page

S. No. (1)	Date (2)	Type III bursts			Flares				
		Start time (UT) (3)	Frequency (MHz)		Time (UT)		Class (8)	Active region (9)	Location (10)
			Start (4)	Stop (5)	Onset (6)	End (7)			
61	20141003	3:04:36	45	179	02:57	03:15	C	12173	S13W85
62	20141009	7:43:13	45	111	07:35	07:51	C	12182	S18W46
63	20141011	4:12:09	45	104	03:26	04:25	B	12187	S13E88
64	20141018	6:50:00	45	176	06:43	06:48	C	12192	S13E72
65	20141021	4:05:18	45	177	04:03	04:07	B	12192	S09E30
66	20141021	8:08:16	45	243	08:08	08:12	C	12192	S09E31
67	20141024	3:55:45	45	107	03:56	04:02	C	12192	S22W00
68	20141027	7:25:58	45	106	07:11	07:20	C	12192	S18W48
69	20141031	9:21:06	45	280	09:19	09:27	C	12201	S02E59
70	20141101	10:22:45	45	220	10:20	10:30	C	12201	S05E47
71	20141102	3:06:28	45	184	03:05	03:11	B	12201	S05E36
72	20141102	5:53:36	45	228	05:41	05:50	B	12201	S05E34
73	20141103	3:47:59	45	360	03:47	03:56	C	12201	S03E21
74	20141103	4:48:34	45	330	04:50	04:56	C	12201	S03E18
75	20141103	7:04:00	45	253	07:06	07:09	B	12201	S03E17
76	20141104	5:25:25	45	111	05:19	05:40	C	12205	N16E84
77	20141108	4:54:31	45	108	05:02	05:10	C	12207	S12E88
78	20141130	5:17:48	45	251	04:52	05:38	C	12222	S18E31
79	20141130	8:42:58	45	404	07:58	09:15	B	12222	S18E29
80	20141201	5:12:59	45	180	05:11	05:22	C	12217	S16W25
81	20141203	2:33:05	45	186	02:30	02:37	C	12217	S16W54
82	20141214	4:26:57	45	156	04:17	04:41	C	12241	S11E74
83	20141214	4:30:29	45	107	04:17	04:41	C	12241	S11E74
84	20141214	6:17:18	45	97	06:19	06:24	C	12227	S02W79
85	20141214	6:21:12	45	166	06:19	06:24	C	12227	S02W79
86	20141214	8:02:41	45	140	08:04	08:12	C	12237	S20E51
87	20141214	8:25:05	45	187	08:25	08:37	C	12237	S18E49
88	20141226	5:31:00	45	186	05:18	05:36	C	12249	S12W37

References

- Benz, A.O., Monstein, C., Meyer, H., Manoharan, P.K., Ramesh, R., Altyntsev, A., Lara, A., Paez, J., Cho, K.-S.: 2009, A World-Wide Net of Solar Radio Spectrometers: e-CALLISTO. *Earth Moon and Planets* **104**, 277. DOI. ADS. [Ben2009]
- Bougeret, J.-L., Kaiser, M.L., Kellogg, P.J., Manning, R., Goetz, K., Monson, S.J., Monge, N., Friel, L., Meetre, C.A., Perche, C., Sitruk, L., Hoang, S.: 1995, Waves: The Radio and Plasma Wave Investigation on the Wind Spacecraft. *Space Sci. Rev.* **71**, 231. DOI. ADS. [Bougeret1995]

- Caroubalos, C., Maroulis, D., Patavalis, N., Bougeret, J.-L., Dumas, G., Perche, C., Alissandrakis, C., Hillaris, A., Moussas, X., Preka-Papadema, P., Kontogeorgos, A., Tsitsipis, P., Kanelakis, G.: 2001, The New Multichannel Radiospectrograph ARTEMIS-IV/HECATE, of the University of Athens. *Experimental Astronomy* **11**, 23. [ADS](#). [[Car2001](#)]
- Ebenezer, E., Subramanian, K.R., Ramesh, R., Sundararajan, M.S., Kathiravan, C.: 2007, Gauribidanur radio array solar spectrograph (GRASS). *Bulletin of the Astronomical Society of India* **35**, 111. [ADS](#). [[Ebe2007](#)]
- Fawcett, T.: 2006, An introduction to roc analysis. *Pattern Recognition Letters* **27**(8), 861. ROC Analysis in Pattern Recognition. [DOI](#). <http://www.sciencedirect.com/science/article/pii/S016786550500303X>. [[Faw2006](#)]
- Gorgutsa, R.V., Gnezdilov, A.A., Markeev, A.K., Sobolev, D.E.: 2001, An upgrade of the izmiran's solar digital radio spectrograph: First results. *Astronomical and Astrophysical Transactions* **20**, 547. [DOI](#). [ADS](#). [[Gor2001](#)]
- Guidice, D.A., Cliver, E.W., Barron, W.R., Kahler, S.: 1981, The Air Force RSTN System. In: *Bulletin of the American Astronomical Society*, *Bulletin of the American Astronomical Society* **13**, 553. [ADS](#). [[Gui1981](#)]
- Hariharan, K., Ramesh, R., Kathiravan, C., Abhilash, H.N., Rajalingam, M.: 2016, High Dynamic Range Observations of Solar Coronal Transients at Low Radio Frequencies with a Spectro-correlator. *Astrophys. J. Supple. Seri.* **222**, 21. [DOI](#). [ADS](#). [[Hariharan2016](#)]
- James, T., Subramanian, P.: 2018, Energetics of small electron acceleration episodes in the solar corona from radio noise storm observations. *Mon. Not. Roy. Astron. Soc.* **479**, 1603. [DOI](#). [ADS](#). [[Jam2018](#)]
- James, T., Subramanian, P., Kontar, E.P.: 2017, Small electron acceleration episodes in the solar corona. *Mon. Not. Roy. Astron. Soc.* **471**, 89. [DOI](#). [ADS](#). [[Jam2017](#)]
- Kaiser, M.L.: 2005, The STEREO mission: an overview. *Advances in Space Research* **36**, 1483. [DOI](#). [ADS](#). [[Kaiser2005](#)]
- Kishore, P., Kathiravan, C., Ramesh, R., Rajalingam, M., Barve, I.V.: 2014, Gauribidanur Low-Frequency Solar Spectrograph. *Solar Phys.* **289**, 3995. [DOI](#). [ADS](#). [[Kis2014](#)]
- Kishore, P., Ramesh, R., Kathiravan, C., Rajalingam, M.: 2015, A Low-Frequency Radio Spectropolarimeter for Observations of the Solar Corona. *Solar Phys.* **290**, 2409. [DOI](#). [ADS](#). [[Kis2015](#)]
- Kondo, T., Isobe, T., Igi, S., Watari, S.-i., Tokumaru, M.: 1994, The New Solar Radio Observation System At Hiraiso. *Communications Research Laboratory Review* **40**, 85. [ADS](#). [[Kon1994](#)]
- Kumari, A., Ramesh, R., Kathiravan, C., Wang, T.J.: 2017, Strength of the Solar Coronal Magnetic Field - A Comparison of Independent Estimates Using Contemporaneous Radio and White-Light Observations. *Solar Phys.* **292**(11), 161. [DOI](#). [ADS](#). [[Ans2017](#)]
- Kundu, M.R.: 1965, *Solar radio astronomy*. [ADS](#). [[Kun1965](#)]
- Lobzin, V.V., Cairns, I.H., Zaslavsky, A.: 2014, Automatic recognition of type III solar radio bursts in STEREO/WAVES data for onboard real-time and archived data processing. *Journal of Geophysical Research (Space Physics)* **119**, 742. [DOI](#). [ADS](#). [[Lob2014](#)]
- Lobzin, V.V., Cairns, I.H., Robinson, P.A., Steward, G., Patterson, G.: 2009, Automatic recognition of type III solar radio bursts: Automated Radio Burst Identification System method and first observations. *Space Weather* **7**, S04002. [DOI](#). [ADS](#). [[Lob2009](#)]
- Lobzin, V.V., Cairns, I.H., Robinson, P.A., Steward, G., Patterson, G.: 2010, Automatic Recognition of Coronal Type II Radio Bursts: The Automated Radio Burst Identification System Method and First Observations. *Astrophys. J. Lett.* **710**, L58. [DOI](#). [ADS](#). [[Lob2010](#)]
- McLean, D.J., Labrum, N.R.: 1985, *Solar radiophysics: Studies of emission from the sun at metre wavelengths*. [ADS](#). [[Mc11985](#)]
- Monstein, C., Ramesh, R., Kathiravan, C.: 2007, Radio spectrum measurements at the Gauribidanur observatory. *Bull. Astron. Soc. India* **35**, 473. [[Monstein2007](#)]
- Mugundhan, V., Hariharan, K., Ramesh, R.: 2017, Solar Type IIIb Radio Bursts as Tracers for Electron Density Fluctuations in the Corona. *Solar Phys.* **292**, 155. [DOI](#). [ADS](#). [[Mug2017](#)]
- Mugundhan, V., Ramesh, R., Kathiravan, C., Gireesh, G.V.S., Hegde, A.: 2018, Spectropolarimetric Observations of Solar Noise Storms at Low Frequencies. *Solar Phys.* **293**(3), 41. [DOI](#). [ADS](#). [[Mug2018](#)]
- Ramesh, R.: 2011, Low frequency solar radio astronomy at the Indian Institute of Astrophysics (IIA). In: *Astronomical Society of India Conference Series, Astronomical Society of India Conference Series* **2**. [ADS](#). [[Ram2011](#)]

- Ramesh, R., Kathiravan, C., Barve, I.V., Beeharay, G.K., Rajasekara, G.N.: 2010, Radio Observations of Weak Energy Releases in the Solar Corona. *Astrophys. J. Lett.* **719**, L41. [DOI](#). [ADS](#). [Ram2010]
- Ramesh, R., Sasikumar Raja, K., Kathiravan, C., Narayanan, A.S.: 2013, Low-frequency Radio Observations of Picoflare Category Energy Releases in the Solar Atmosphere. *Astrophys. J.* **762**, 89. [DOI](#). [ADS](#). [Ram2013]
- Rucker, H.O., Macher, W., Fischer, G., Oswald, T., Bougeret, J.L., Kaiser, M.L., Goetz, K.: 2005, Analysis of spacecraft antenna systems: Implications for STEREO/WAVES. *Advances in Space Research* **36**, 1530. [DOI](#). [ADS](#). [Rucker2005]
- Saint-Hilaire, P., Vilmer, N., Kerdraon, A.: 2013, A Decade of Solar Type III Radio Bursts Observed by the Nançay Radioheliograph 1998-2008. *Astrophys. J.* **762**, 60. [DOI](#). [ADS](#). [Sai2013]
- Salmane, H., Weber, R., Abed-Meraim, K., Klein, K.-L., Bonnin, X.: 2018, A method for the automated detection of solar radio bursts in dynamic spectra. *Journal of Space Weather and Space Climate* **8**(27), A43. [DOI](#). [ADS](#). [Sa12018]
- Sasikumar Raja, K., Ramesh, R.: 2013b, Low-frequency Observations of Transient Quasi-periodic Radio Emission from the Solar Atmosphere. *Astrophys. J.* **775**, 38. [DOI](#). [ADS](#). [Sas2013b]
- Sasikumar Raja, K., Kathiravan, C., Ramesh, R., Rajalingam, M., Barve, I.V.: 2013a, Design and Performance of a Low-frequency Cross-polarized Log-periodic Dipole Antenna. *Astrophys. J. Supple. Seri.* **207**, 2. [DOI](#). [ADS](#). [Sas2013a]
- Sasikumar Raja, K., Subramanian, P., Ananthakrishnan, S., Monstein, C.: 2018, CALLISTO Spectrometer at IISER-Pune. *ArXiv e-prints*. [ADS](#). [Sas2018]
- Sharma, R., Oberoi, D., Arjunwadkar, M.: 2018, Quantifying Weak Nonthermal Solar Radio Emission at Low Radio Frequencies. *Astrophys. J.* **852**, 69. [DOI](#). [ADS](#). [Roh2018]
- Tarnstrom, G.L., Philip, K.W.: 1972, Solar Radio Spike Bursts. *Astron. Astrophys.* **16**, 21. [ADS](#). [Tar1972]
- Wild, J.P.: 1967, The Radioheliograph and the Radio Astronomy Programme of the Culgoora Observatory. *Proceedings of the Astronomical Society of Australia* **1**, 38. [DOI](#). [ADS](#). [Wild1967]
- Zhang, P.J., Wang, C.B., Ye, L.: 2018, A type III radio burst automatic analysis system and statistic results for a half solar cycle with Nançay Decameter Array data. *Astron. Astrophys.* **618**, A165. [DOI](#). [ADS](#). [Zha2018]